IEEE Access
Multidisciplinary ⋮ Rapid Review ⋮ Open Access Journal

Received July 19, 2020, accepted September 2, 2020, date of publication September 8, 2020, date of current version September 22, 2020.

Digital Object Identifier 10.1109/ACCESS.2020.3022651

Numerical Investigation on Hydrodynamic Characteristics of Landslide-Induced Impulse Waves in Narrow River-Valley Reservoirs

BIN DENG[1,2,3], HE TAO[1], CHANGBO JIANG[1,2,3], AND KE QU[1,2,3]

[1]School of Hydraulic Engineering, Changsha University of Science and Technology, Changsha 410114, China
[2]Key Laboratory of Dongting Lake Aquatic Eco-Environmental Control and Restoration of Hunan Province, Changsha University of Science and Technology, Changsha 410114, China
[3]Key Laboratory of Water-Sediment Sciences and Water Disaster Prevention of Hunan Province, Changsha University of Science and Technology, Changsha 410114, China

Corresponding author: Ke Qu (qukeforjc@126.com)

This work was supported in part by the National Natural Science Foundation of China under Grant 51979015, Grant 51879015, and Grant 51809021, in part by the Natural Science Foundation of Hunan Province, China, under Grant 2018JJ3535, and in part by the Transportation Science and Technology Foundation of Qinghai Province under Grant 2014-09. The work of Bin Deng was supported in part by the China Scholarship Council.

ABSTRACT Landslide-induced impulse waves in a river-valley reservoir region have become a serious threat to life and property intactness. Compared with previous studies focusing on landslides in open-water regions, this article systematically carried out numerical investigations on the hydrodynamic characteristics of landslide-induced impulse waves in narrow river-valley reservoirs by applying software package FLOW3D. To verify the computational reliability of FLOW3D, necessary experimental work was conducted. The predicted temporal evolutions of water elevation at selected wave gauges are in good agreement with that recorded during the corresponding experiment. The effects of some prominent factors, such as the drop height of the slide, still-water depth, slide volume, and slide slope, on the propagation and magnitude of landslide-induced impulse waves are investigated in detail by systematically analyzing both simulation and experimental results. Based on simulation results, we proposed empirical formulas for predicting the landslide-induced impulse waves by performing dimensionless analysis and applying nonlinear regression methods. Then, the proposed empirical formulas were applied to predict the impulse waves induced by four landslide accidents. It is believed that the findings drawn from this article could greatly enhance our understanding on the hydrodynamic characteristics of landslide-induced impulse waves in narrow river-valley reservoir regions, and the proposed empirical formulas can be used as quick technical support for the safe navigation of such rivers.

INDEX TERMS Landslide, river-valley reservoir, impulse waves, hydrodynamics.

I. INTRODUCTION

Landslide-induced impulse waves with large volume and high velocity have become a serious potential threat to the safety of riverside residents and the intactness of navigation vessels in the river-valley reservoir region, characterized by narrow reservoir geometries and steep shores. During the past few decades, many river reservoirs have been gradually constructed in the mountainous areas, directly causing serious riverbank-slope instability problems, and the reservoir regions have become significantly vulnerable to landslides, especially under the influence of long-period high-water-level conditions and regular reservoir operations. Compared with landslides in open-water regions, landslides in narrow river-valley reservoir regions can generate impulse waves with greater transverse and longitudinal propagation, resulting in worse consequences. There are many examples of significant damage to infrastructure, especially large reservoirs and dams, due to serious landslide-induced impulse waves that happened in water-conservancy construction projects around the world. For example, at 22:39 of October 9th 1963, a massive landslide that occurred in the Vajont reservoir in Italy caused a tragic event that shocked the world. The volume of the landslide body was 260 million m^3, which generated

The associate editor coordinating the review of this manuscript and approving it for publication was Jenny Mahoney.

(a)

(b)

FIGURE 1. Typical landsides in the Wushan area. (a) Landslide accident in Yangtze River; (b) damaged port and ships.

huge impulse waves, 250 m in height at the opposite shore, and the impulse waves cross over the top of dam, leading to about 2000 deaths and the complete destruction of several villages and towns [1], [2]. In June 2015, a 6 m high impulse-wave was generated by a 24,000 m^3 Wushan landslide that fell into the Yangtze River in Chongqing, China. It resulted in the sinking of 21 small ships berthing on the opposite side Fig. 1, and at least one death and five injuries [3], [4]. Therefore, it is necessary to understand the underlying physics during the process of impulse waves generation, propagation, and their final impact on infrastructure, as well as attenuation for proper site selection for wharfs and safer navigation-route design in river-valley reservoir regions.

In the past, hydrodynamic characteristics of landslide-induced impulse waves in open-water regions have been extensively studied by many researchers through theoretical [5], [6], experimental [1], [7], [8], and numerical approaches [9]–[11], focusing on impulse-wave height and propagation characteristics. Regarding the theoretical studies, Noda *et al.* [12] simplified the landslide problem into horizontal or vertical landslides, and derived analytical solutions by using linear approximation and infinite approximation, respectively. By applying the wavelet-transform method, Panizzo *et al.* [13] analyzed the evolution of impulse waves height induced by landslides. Using linear theory, Risio and Sammarco [14] derived a new analytical solution to study the propagation law of impulse waves, which can predict the height and period of impulse waves For the experimental work, Heller and Hager [15] studied the generation and propagation of impulse waves induced by bulk landslides by carrying out a flume experiment, revealing the seven prominent factors determining the maximum impulse-wave height. Since a landslide-induced impulse-wave has extremely strong three-dimensional (3D) characteristics, a two-dimensional (2D) flume experiment has inherited drawbacks. Zweifel and Hager [16], and Fritz [17] carried out a series of 2D experiments on impulse waves induced by artificial granular material entering water in the Hydraulic Laboratory (VAW) of Zurich University (ETH). They also derived analytical formulas for predicting the propagation of impulse waves and the corresponding wave period. Enet *et al.* [39] Studied landslide impulse wave caused by underwater rigid-body landslides through large-scale three-dimensional experiments. A high-speed camera is used to record the trajectory of the landslide body. The miniature accelerometer in the landslide model measures the acceleration of the landslide body. The analytical law of the landslide motion is deduced from the measurement data, and the dispersion and nonlinear effects of the impulse-wave are analyzed. Zu *et al.* [18] established a four-dimensional mathematical model among wave-height transmissibility rate, initial wave height, water depth, and azimuth angle, as well as propagation distance, through utilizing the tensor space-mapping method. They summarized the general regularity of the propagation and attenuation of landslide-induced impulse waves. Their findings can be applied to analyze and forecast a landslide-induced impulse waves, and scientifically and accurately determine the damage range of landslide-induced impulse waves. Along with experimental studies, numerical investigation has become increasingly popular, and various numerical models have been established to study the hydrodynamic characteristics of landslide-induced impulse waves. Based on the methods reported by Yin *et al.* [19] and Grilli *et al.* [20] modified the seabed landslide-generated surge-source model to form an initial source model for underwater landslide-generated impulse waves; this improved model can be used to predict potential impulse waves disasters at different water levels in mountainous reservoir areas. Mao *et al.* [21] developed a three-phase finite-element numerical model to evaluate the devastating hazards of landslide-induced impulse waves, due to huge energy-carrying capability during the process of impulse waves generation and propagation. Recently, Huang *et al.* [22] established a fully coupled numerical model for landslide-induced impulse waves based on the noncoherent granular flow-governing equation. This has been used to analyze the characteristics of the landslide motion and

generated impulse waves, and predict the final deposition and wave run-up height.

It is not hard to find that earlier studies mainly focused on the study of wave type, shape change, maximum impulse waves height, and propagation characteristics caused by the landslide entering the water. Among them, the study on maximum impulse waves height and wave-velocity characteristics caused by the landslide entering the water in the cross section of the river channel is relatively common. Some people pointed out that the height of an impulse waves depends mainly on landslide volume and Froude number [12], [23]. Subsequently, some scholars further studied the effects of slope, water depth, landslide-body size, and shape-to-swell height, and derived a series of empirical formulas [24], [25]. In addition, Zhang *et al.* [40] Used the ''Tsunami squared'' numerical method to study the effect of reservoir width changes in the Three Gorges Reservoir area on landslide impulse-wave propagation. Compared with the convergent reservoir, the divergent reservoir geometry has a greater effect on wave propagation attenuation. Heller *et al.* [42] obtained the maximum amplitude, wave height, period and along the propagation deformation equation through the experiment of 144 slides under the three parameter system changes of Froude number, relative slide mass and slide thickness.

Obviously, the current landslide-wave model tests can comprehensively consider influencing factors such as landslide shape, velocity, landslide volume, and water depth. However, the study on the influence of channel configuration on the impulse waves has not been thoroughly carried out. Most river-landslide models are established for relatively wide rivers. Very limited research has been carried out to investigate the hazard potential of landslide-induced impulse waves in narrow river-valley reservoirs of mountainous areas. The generating and propagating phenomena of landslide-induced impulse waves in narrow river-valley reservoir regions are significantly different from those in open-water regions, since the propagation of impulse waves can be greatly influenced by strong reflected waves formed at the opposite riverbank, making the generation mechanism of landslide-induced impulse waves more complicated. Therefore, it is now urgently needed to meet the knowledge gap on landslide-induced impulse waves in narrow river-valley reservoirs and their hydrodynamic influence in the surrounding environment.

In this study, to enhance our understanding on landslide-induced impulse waves in narrow river-valley reservoir regions, a series of experimental work was conducted. In addition, with the development of CFD technology, more and more research work adopts CFD technology [9]–[11], [43], software package FLOW-3D, as a 3D two-phase flow model was applied to systematically study the generation and propagation of landslide-induced surge waves in narrow reservoir river regions at a laboratory scale, and it has been approved to be effective research tools for studies on landslide-induced impulse waves [26]–[30]. In present paper, 3D experimental data is used to verify the reliability of our 3D numerical model (FLOW-3D). Then, the simulation results of the verified 3D numerical model have been used to derive our empirical formulas in predicting impulse waves in both lateral and longitudinal directions. For landslide accidents happened in the narrow river-valley reservoir regions, we apply the limited measured results to further verify the reliability of our empirical formula in predicting impulse waves in real-scale landslide problem. The rest of the paper is organized as follows. Governing equations and corresponding numerical methods of the software packages, model validations are described in Section 2. Section 3 discusses the hydrodynamic characteristics of the generation and propagation of landslide-induced impulse waves, and proposes empirical formulas for predicting the initial maximum surge height, and longitudinal and lateral attenuation based on both experimental and numerical results. Moreover, Section 3 further verifies the accuracy and reliability of the proposed empirical formulas by performing four landslide accidents. The main conclusions drawn from this study are listed in Section 4.

II. METHODS

The 3D landslide-induced impulse-wave model is established using the full three-dimensional commercial code Flow-3D (Flow Science, Inc., Santa Fe, NM). The model has been widely applied to study the characteristics of impulse-wave generation and propagation caused by landslides into reservoirs [29], [30]. The model solves the Reynolds-Averaged Navier–Stokes Equations and the continuity equation for incompressible flow along with the true volume-of-fluid method (VOF, Hirt and Nichols, 1981) in order to compute free-surface motion. The general moving-object module (GMO) was selected to simulate the interaction between moving objects and the fluid for the purpose of modelling landslide-generated waves. Source terms were added in the continuity equation and the VOF transport equation in order to describe the hydrodynamic effects of moving objects. In particular, shear velocity at the moving-object boundaries is accounted for into shear-stress terms in momentum equations (Flow Science, 2007). Therefore, the resulting general 3D continuity and momentum equations considering fluid motion, GMO motion, the viscosity of the fluid, and porous media are:

$$\frac{\partial}{\partial x}(uA_x)+\frac{\partial}{\partial y}(vA_y)+\frac{\partial}{\partial z}(wA_z)=\frac{R_{SOR}}{\rho} \tag{1}$$

$$\left.\begin{aligned}
&\frac{\partial u}{\partial t}+\frac{1}{V_F}\left\{uA_x\frac{\partial u}{\partial x}+vA_y\frac{\partial u}{\partial y}+wA_z\frac{\partial u}{\partial z}\right\}\\
&\quad=-\frac{1}{\rho}\frac{\partial p}{\partial x}+G_x+f_x-b_x-\frac{R_{SOR}}{\rho V_F}(u-u_w-\delta u_s)\\
&\frac{\partial v}{\partial t}+\frac{1}{V_F}\left\{uA_x\frac{\partial v}{\partial x}+vA_y\frac{\partial v}{\partial y}+wA_z\frac{\partial v}{\partial z}\right\}\\
&\quad=-\frac{1}{\rho}\left(R\frac{\partial p}{\partial y}\right)+G_y+f_y-b_y-\frac{R_{SOR}}{\rho V_F}(v-v_w-\delta v_s)\\
&\frac{\partial w}{\partial t}+\frac{1}{V_F}\left\{uA_x\frac{\partial w}{\partial x}+vA_y\frac{\partial w}{\partial y}+wA_z\frac{\partial w}{\partial z}\right\}\\
&\quad=\frac{1}{\rho}\frac{\partial p}{\partial z}+G_z+f-b_z-\frac{R_{SOR}}{\rho V_F}(w-w_w-\delta w_s)
\end{aligned}\right\} \tag{2}$$

In Equation (1), ρ is the density of water, (A_x, A_y, A_z) are the fraction areas of fluids in the x, y, and z directions, (u, v, w) are the velocity components in the x, y, and z directions, and R_{SOR} is a mass source. The mass-source term, when the FAVOR (Fractional Area Volume Obstacle Representation) is used, also accounts for the additional volume source generated on the boundary of a moving object. In Equation (2) V_F is the fraction volume open to flow, (G_x, G_y, G_z) are the gravitational acceleration in the x, y, and z directions, (f_x, f_y, f_z) are the viscous terms in the x, y, and z directions, and (b_x, b_y, b_z) are flow losses in porous media. The final terms account for the injection of mass at a source represented by a geometry component; in fact, the term (u_w, v_w, w_w) represents the velocity of the source component that is generally nonzero for a mass source at a GMO. The term (u_s, v_s, w_s) is the fluid velocity at the surface of the source relative to the source itself.

Fluid configurations are defined in terms of a VOF function, F (x, y, z, t), which represents the volume of fluid per unit volume and satisfies the equation:

$$\left[\frac{\partial}{\partial x}(FA_x u) + \frac{\partial}{\partial y}(FA_y v) + \frac{\partial}{\partial z}(FA_z w)\right] = F_{DIF} + F_{SOR} \quad (3)$$

F_{DIF} is a different diffusion term for two-fluid mixing, and the term F_{SOR} is the time rate of change of the volume fraction of fluid associated with the mass source.

In the above model, the RNG k-ε turbulence model [34], [35] was implemented as the turbulence closure, the second-order finite-difference method was utilized to discretize the momentum equations, the TruVOF [31], [32] method was used to capture the interface between air and water, and the pressure and velocity was coupled by GMRES Pressure-Velocity Solvers [33].

A. MODEL SETUP AND VALIDATION

1) EXPERIMENTAL SETUP

Experiments were carried out in the Key Laboratory of Water and Sediment Science and Water Disaster Prevention and Control in Hunan Province at the Changsha University of Science and Technology. The wave flume was 1.8 m in height, 1.5 m in width, and 60 m in length (60m × 1.5m × 1.8m). The experimental layout is depicted in Fig. 2, which represents a typical layout for a landslide accident near a dam reservoir region with a scale ratio of about 1:200. As observed in Fig. 2a, the configuration of the slide was cuboid with 0.2 m in length and 0.1 m in width. The model is based on the Froude similarity rule, so other similarity ratios can be obtained as shown in table 3. In the experimental work, the density of the slide was 2560 kg/m^3, and the volume of the slide could be directly adjusted by varying its thickness or height. As shown in Fig. 2, the wave height was recorded by eight gauges. Three of them were arranged transversely with wave-gauge G1 locating in the middle of the domain. Wave-gauge G4 was used to measure the run-up height of the impulse waves. Six wave gauges were arranged longitudinally. As reported in Fritz [17], the slide would

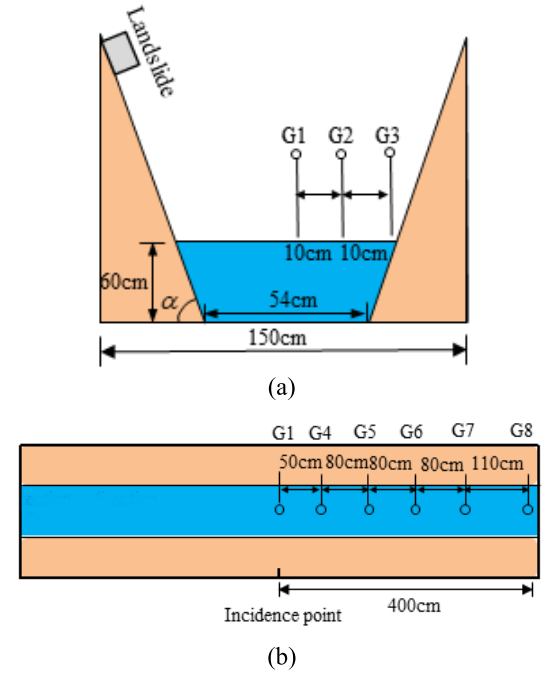

FIGURE 2. Experimental layout. (a) Side view and (b) top view.

readily collapse, if the slope of the riverbank were in the 60 to 90 degrees range. Hence, we set the bank slope at 75 degrees. Other parameters designed for different experimental runs are listed in Table 1. In the present paper, each experimental run was repeated five times, and the recorded data were averaged to satisfy accuracy requirements and reduce possible experimental errors.

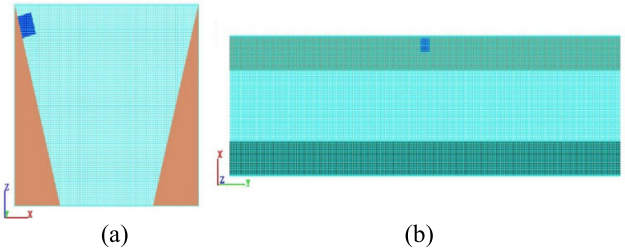

FIGURE 3. Mesh layout for computation. (a) Side view and (b) top view.

2) NUMERICAL SETUP

The computational domain was 8 m in length, 1.5 m in width, and 1.8 m in height. A high-resolution computational mesh with 2 million grids was generated to resolve the free-surface profile in high fidelity, as shown in Fig. 3. Simulation duration was 8 s. To meet the numerical-stability requirement, an adaptive time step was selected. In addition to the value of the slope used in the experimental work, three more bank slopes were selected: 30, 35, and 40 degrees. Table 2 lists the parameter setup for all simulation runs. These simulation runs were designed to systematically analyze the influence

TABLE 1. Parameters for each landslide events.

Parameters	Slide volume V(cm^3)	Drop height H(m)	Water Depth h(m)	Slide Slope β(°)
E1	1600	0.8	0.6	75
E2	2000	0.8	0.6	75
E3	2500	0.8	0.6	75
E4	2000	1.0	0.6	75
E5	2000	1.2	0.6	75
E6	2000	1.4	0.6	75
E7	2000	0.8	0.4	75
E8	2000	0.8	0.5	75
E9	2000	0.8	0.7	75
E10	3000	1.2	0.5	75
E11	4500	1.2	0.5	75
E12	2250	1.2	0.5	75
E13	1500	1.2	0.5	75
E14	3000	1.3	0.5	75
E15	3000	1.4	0.5	75
E16	3000	1.5	0.5	75
E17	3000	1.2	0.6	75
E18	3000	1.2	0.7	75

TABLE 2. Parameter setup for numerical simulation.

Parameters	Slide Volume V(cm^3)	Drop height H(m)	Water Depth h(m)	Slide Slope β (°)
S1	1600	0.8	0.6	35
S2	2000	0.8	0.6	35
S3	2500	0.8	0.6	35
S4	3000	0.8	0.6	35
S5	2000	1.0	0.6	35
S6	2000	1.2	0.6	35
S7	2000	1.4	0.6	35
S8	2000	0.8	0.4	35
S9	2000	0.8	0.5	35
S10	2000	0.8	0.7	35
S11	2000	0.8	0.6	30
S12	2000	0.8	0.6	40
S13	2000	0.8	0.6	75

of prominent factors, such as falling, on the generation and spread of landslide-induced impulse waves.

3) NUMERICAL SETUP MODEL VALIDATION

In this section, the computational capability of our numerical model in predicting landslide-induced impulse waves is validated by reproducing experimental runE2, describe in the experimental setting section. Fig. 4 plots the comparison of the time series of water elevation between prediction and measurement recorded at three selected wave gauges. As observed in Fig. 4, they are in good agreement with respect to wave period and wave height. To further verify the accuracy of the computation, the skill number was calculated using Equation (4) [36]:

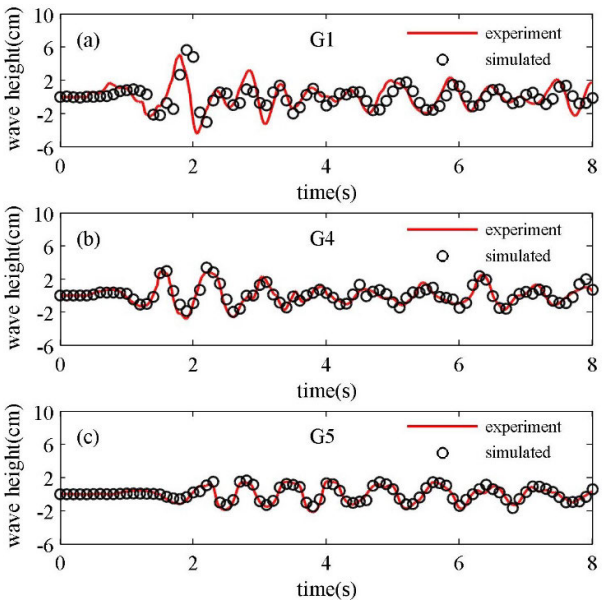

FIGURE 4. Comparison of time series of water elevation recorded at different wave gauges under S13. (a) Gauge 1; (b) Gauge 4; and (c) Gauge 5.

$$skill = 1 - \frac{\sum \left|X_{unm} - X_{exp}\right|^2}{\sum \left(\left|X_{unm} - \overline{X_{exp}}\right| + \left|X_{exp} - \overline{X_{exp}}\right|\right)^2} \quad (4)$$

where X_{num} and X_{exp} represent predictions and measurements, respectively. It appeared that the skill numbers for all water-elevation comparisons plotted in Fig. 4 were greater than 0.9. The difference between measurement and simulation results at G1 alone was relatively noticeable, which can be due to complicated wave interactions, especially the reflected wave from the opposite channel shore. Based on the results demonstrated above, our numerical model could simulate hydrodynamic characteristics of an impulse-wave well and with high accuracy.

III. RESULTS AND DISCUSSION

A. HYDRODYNAMICS OF LANDSLIDE-INDUCE IMPULSE WAVES

This section describes the hydrodynamic characteristics of landslide-induced impulse waves in detail. The simulation result for S13 is demonstrated and discussed in this section. Fig. 5 shows snapshots of the water body at different time instances during the process of impulse-wave generation, propagation, run-up, and recession from the opposite

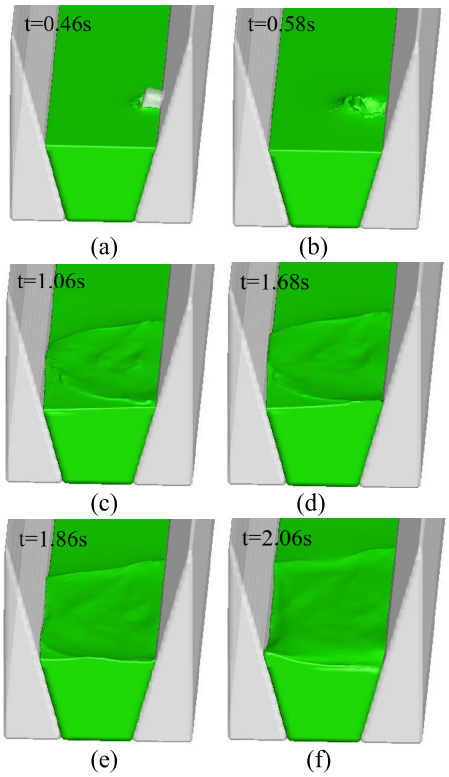

FIGURE 5. Snapshots of water-body contour for an impulse-wave at different time instances: (a) t = 0.46s; (b) t = 0.58s; (c) t = 1.60s; (d) t = 1.68s; (e) t = 1.86s; and (f) t = 2.06s.

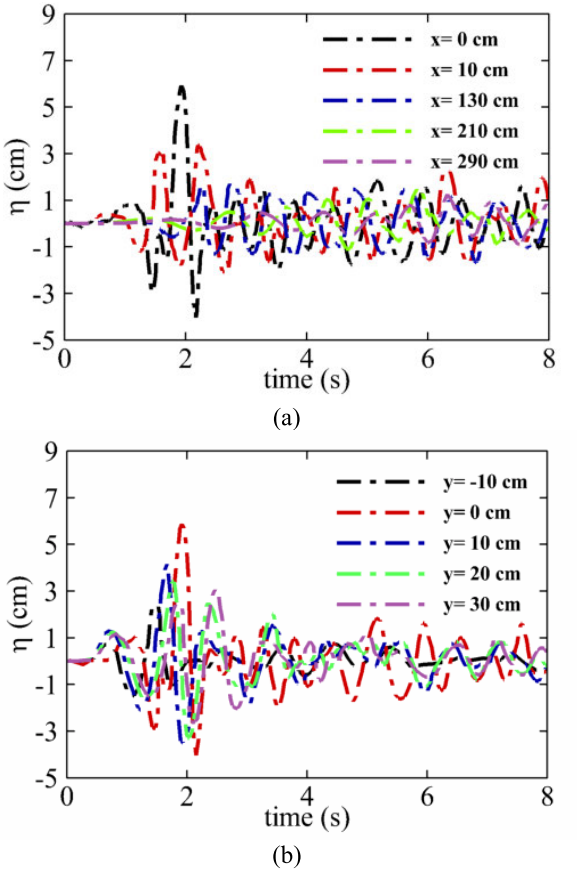

FIGURE 6. Time series of water elevation recorded at selected wave gauges. (a) Longitudinal direction; (b) lateral direction.

channel shore. As seen in Fig. 5, the temporal evolution of the landslide-induced impulse waves can generally be summarized as three stages:

1) During the first stage, the water body is squeezed to spread around the entering site. As shown in Fig. 5a, just when the slide enters the water body, a impulse-wave bore traveling forward is generated in a very short time, behaving as an impact-wave. At t = 0.58 s, after the slide completely enters the water body, it replaces the volume of the original water body, causing the surrounding water body to rise up, as observed in Fig. 5b.

2) Propagation and attenuation of the impulse waves occur during the second stage. After t = 1.6s, the impulse-wave spreads laterally to reach the opposite channel shore Fig. 5c. Meanwhile, it also gradually propagates along the channel in a longitudinal direction. The intensity of impulse waves can be attenuated to some extent due to the viscous effects of the water Fig. 5d.

3) In the third stage, the impulse-wave runs up onto the opposite channel shore Fig. 5e. Once the landslide-induced impulse-wave reaches its maximum run-up height, it retreats under the influence of gravity Fig. 5f.

Fig. 6 plots the temporal evolution of water elevation recorded at five selected wave gauges arranged in both the longitudinal and lateral directions, where η is the impulse - wave height. As observed in Fig. 6a, impulse-wave height gradually decreases with the distance measured from the slide entering the site in the longitudinal direction. The attenuation rate of the impulse-wave also decreases with distance. In addition, it is observed that the attenuation rate of impulse waves in the lateral direction is slightly attenuated with distance compared with that in the longitudinal direction Fig. 6b. This is possibly due to the narrow river reach and the relatively large slide volume. Furthermore, when the wave gauge is located close to the slide entering the site (y = 10 cm), the wave height also is slightly lower than other measuring points.

B. EFFECT OF PROMINENT FACTORS

1) INITIAL MAXIMUM IMPULSE-WAVE HEIGHT IN THE LATRAL DIRECTION

In this section, the effects of prominent factors, such as drop height (H), on the variation of the initial maximum wave height of landslide-induced impulse waves are discussed in detail. Fig. 7 shows the initial maximum wave height as function of slide volume, drop height, slide slope, and water depth. And Fig. 8 also shows the relationship between initial maximum wave height and relevant parameters. It can be seen that wave height increases almost linearly with slide volume (Fig. 7a and Fig. 8a). This is because an increase in slide volume can greatly enlarge both the final kinetic energy

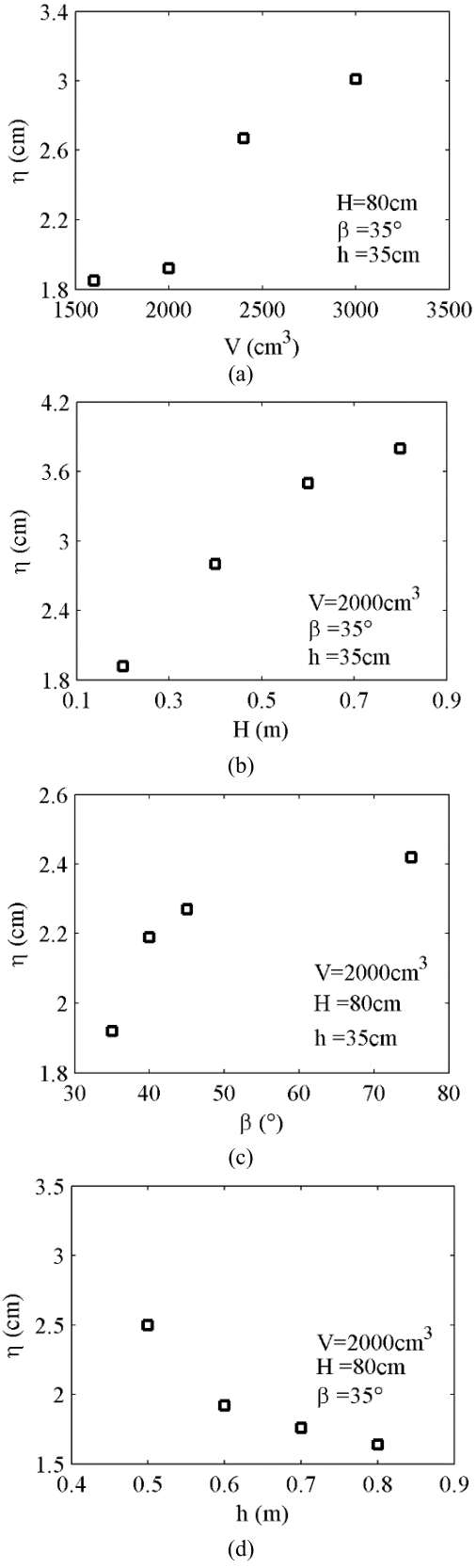

FIGURE 7. Numerical results for the initial maximum impulse-wave height as function of (a) slide volume (V); (b) drop height (H); (c) slide slope (β); and (d) water depth (h).

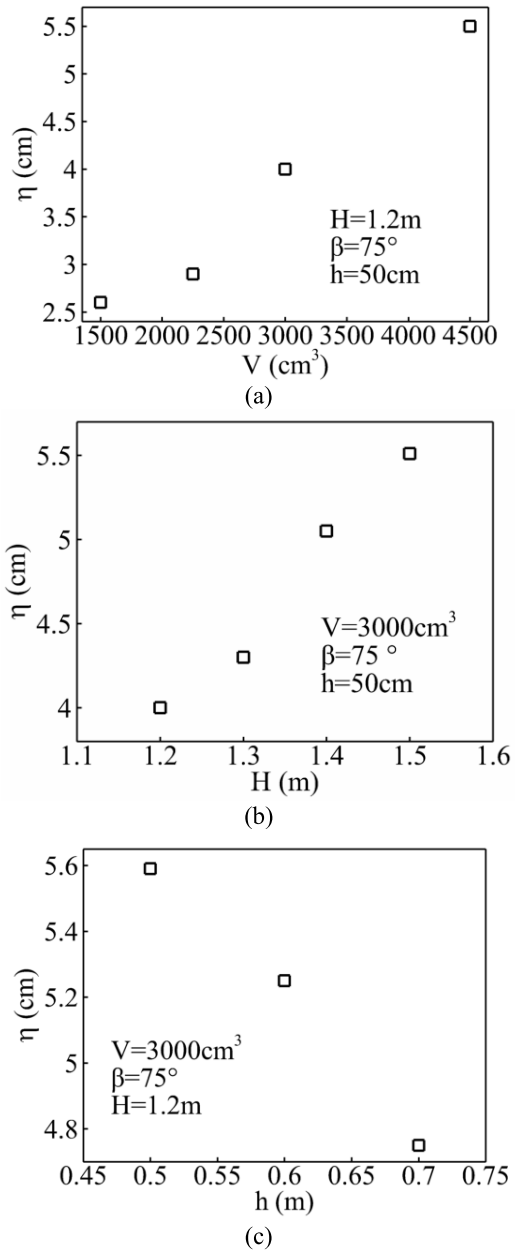

FIGURE 8. Experimental results for the initial maximum impulse-wave height as function of (a) drop height (H); (b) slide volume (V); (c) water depth (h).

of the slide and the contact surface area between the slide and the water. As observed in Fig. 7b and Fig. 8b, impulse-wave height also increases linearly with the increasing of the drop height of the slide. Since an increase in the slide slope can significantly reduce the magnitude of frictional force between the surface of the slide and the sliding plane, resulting in higher final kinematic energy for the slide before it enters the water, wave height increases with increasing slide slope Fig. 7c. As seen fromFig. 7d and Fig. 8c, wave height gradually decreases with still-water depth. It is due to this reason that increasing the water depth will reduce

the drop height of the slide, thus the energy will be reduce which the slider kinetic energy is converted into a wave energy. In addition, an increase in still-water depth results in an increase in the surface area of the reservoir. Hence, the energy-carrying capability by unit width of the water body increases, and landslide-induced impulse-wave height decreases. This can become more obvious for narrow river-valley reservoirs, since any change in still-water depth can cause the width of the reservoir area to rapidly change when the slope of the river shore is large.

2) CHARACTERISTICS OF WAVE PROPAGATION IN THE LONGITUDINAL DIRECTION

In this section, we discuss the hydrodynamic characteristics of the propagation of landslide-induced impulse waves in the longitudinal direction. Variations of the maximum impulse-wave height of a landslide-induced impulse-wave as function of slide volume, drop height, slide slope, and still-water depth along the centreline of the channel are plotted in Fig. 9. As can be seen from Fig. 9a, the larger the slide volume is, the higher the impulse wave can be. Meanwhile, wave height gradually decreases with the longitudinal distance measured from the entering site of the slide while the reducing rate of the maximum impulse-wave height decreases. Basically, similar to the maximum impulse-wave height under different slide volumes, the maximum impulse-wave height gradually increases with the drop height Fig. 9b. It is also observed that the attenuation rate of impulse-wave height is very high, with a distance of 0.5m. For instance, as an impulse-wave propagates from x = 0.5 to x = 1.3 m, the maximum impulse-wave height reduces from 1.64 to 0.86 cm. However, the attenuation rate of the impulse wave reduces greatly when the impulse waves propagates from x = 2.1 to x = 2.9 m, since the maximum height of the impulse wave only reduces from 0.84 to 0.51 cm. Variations of impulse-wave height under different bank slopes along the centreline of the channel are plotted in Fig. 9c. As observed in Fig. 9c, the bank slope has very limited influences on the propagation of impulse waves in a longitudinal direction. Fig. 9d demonstrates the variation of maximum impulse-wave height under different still-water depth. As seen from Fig. 9d, maximum impulse-wave height decreases with still-water depth, especially when still-water depth increases from 0.4m to 0.6 m.

3) LATERAL WAVE PROPAGATION

The hydrodynamic characteristics of impulse-wave propagation in the lateral direction are discussed in this section. Fig. 10 depicts variations of maximum impulse-wave height in the lateral direction as function of slide volume, drop height slide slope, and still water depth. Variation of maximum impulse-wave height under different slide volumes is plotted in Fig. 10a. It shows that the larger the slide volume is, the greater the impulse waves height will be. The attenuation rate of an impulse-wave within a lateral distance of 0.1 m is relatively large. The maximum attenuation rate of wave

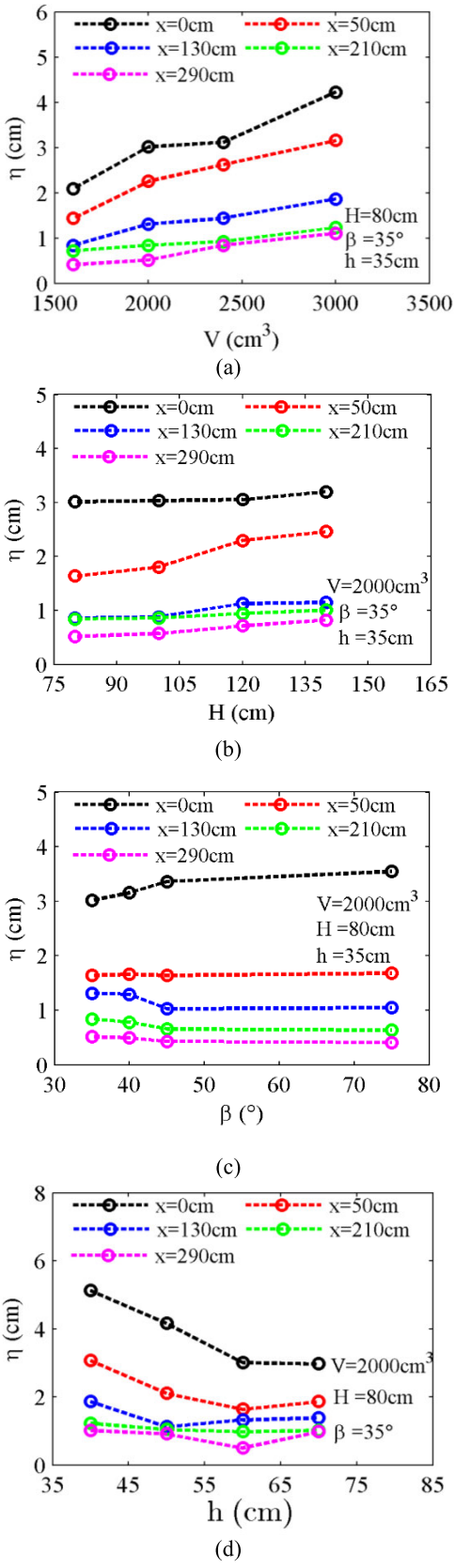

FIGURE 9. Numerical results for the variation of the maximum impulse-wave height in the longitudinal direction as function of (a) slide volume (V); (b) drop height (H); (c) slide slope (β); and (d) water depth (h).

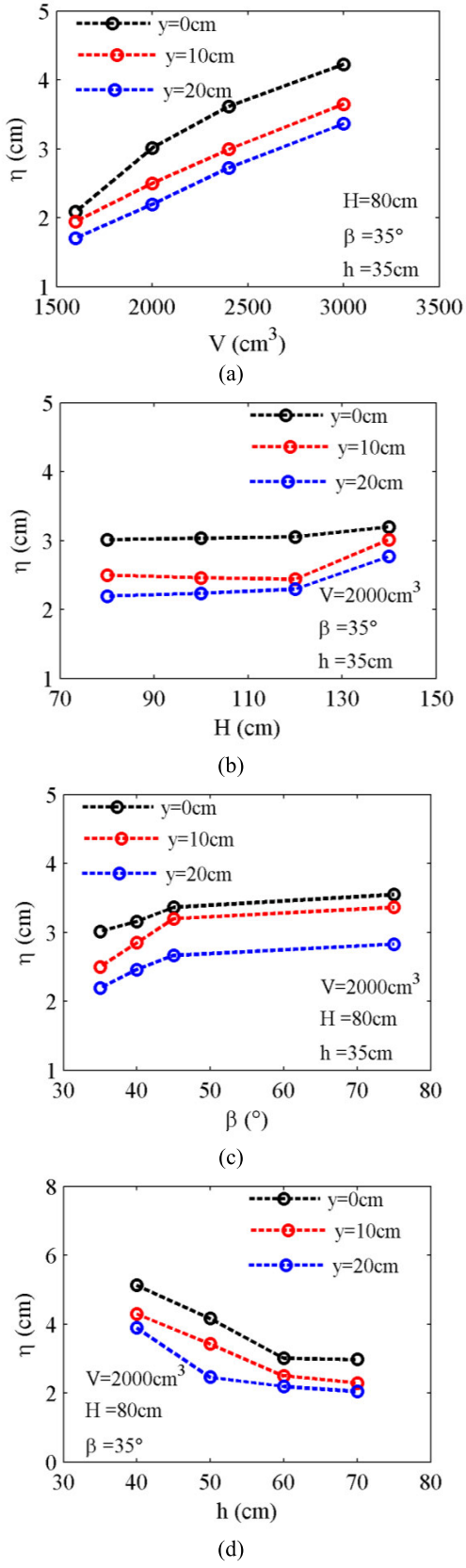

FIGURE 10. Numerical results for the variation of the maximum impulse-wave height in lateral direction as function of (a) slide volume (V); (b) drop height (H); (c) slope (β); (d) water depth (h).

height within the first lateral distance of 0.1 m is about 17%. It was also found that the drop of the slide had very limited influence on the maximum impulse-wave height along the center line of the channel, but it did have noticeable influence on the maximum impulse-wave height when the drop of the slide was larger than 0.12 m Fig. 10b. Similar to the variation of maximum impulse-wave height in the longitudinal direction, the maximum impulse-wave height increases with the slide slope Fig. 10c, but decreases with still-water depth Fig. 10d.

C. EMPIRICAL FORMULAS FOR LANDSLIDE-INDUCED IMPULSE WAVES

In this section, based on the simulation results presented above, we derive the empirical formulas for predicting initial maximum impulse-wave height and evaluating the attenuation of an impulse wave in both longitudinal and lateral directions by performing dimensionless analysis and applying nonlinear regression methods [37], [38]. The initial maximum impulse-wave height can be calculated with Equation (5), which systematically considers the influence of slide volume, drop height, slide slope, and still-water depth.

$$\frac{\eta_{\max}}{h} = 0.287\left(\frac{H}{h}\right)^{1.027}\left(\frac{V}{h^3}\right)^{0.335}\sin\beta^{0.147} \tag{5}$$

Comparison of the predicted initial maximum impulse-wave height and the calculations by Equation (5) is plotted in Fig. 11. Corresponding correlation-coefficient R^2 is 0.925, indicating the reliability of Equation (5). Hence, we can use Equation (5) as a technical tool to make fast predictions of the initial maximum impulse-wave height by comprehensively reflecting the influences of slide volume, drop height, slide slope, and still-water depth.

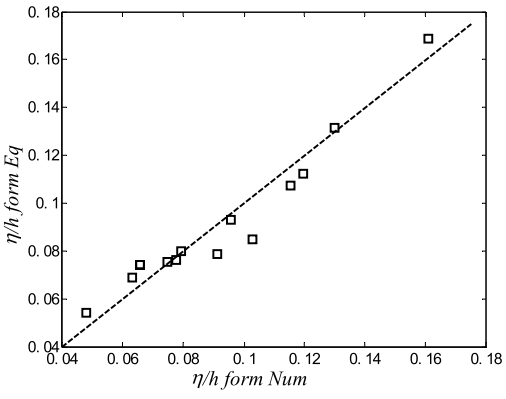

FIGURE 11. Comparison of the predicted initial maximum impulse-wave height by numerical simulation and the calculations by Equation (5).

Liu [38] proposed a theoretical formula for the rapid estimation of the attenuation of a landslide-induced impulse-wave in the Three Gorges reservoir area, as follows:

$$\eta_r(x,t) = \eta_0 e^{-\sqrt{\frac{q}{h_0\eta_0}}x-\sqrt{\frac{g}{\eta_0}}t} \tag{6}$$

where η_r is the wave height in the longitudinal direction, η_0 is the initial maximum impulse-wave height, h is the still-water depth of the reservoir area, x is the distance measured from the entering site of the slide, and p and q are constants.

In this article, to systematically consider the joint influences of slide volume, drop height, slide slop, and still-water depth, we derive a formula by adapting Liu's formula, as follows:

$$\frac{\eta_r}{h} = a(\frac{H}{h})^b(\frac{V}{h^3})^c \sin\beta^d e^{-\sqrt{p}\frac{x}{h}} \quad (7)$$

where a, b, c, d, and p are constants. By applying the regression method, the following empirical formula is derived based on simulation results:

$$\frac{\eta_r}{h} = 1.857(\frac{H}{h})^{0.131}(\frac{V}{h^3})^{0.78} \sin\beta^{0.073} e^{-\sqrt{0.125}\frac{x}{h}} \quad (8)$$

Fig. 12 plots the comparison of predicted impulse-wave heights in the longitudinal direction and the calculations by Equation (8). As seen from Fig. 12, the empirical formula has good accuracy in predicting variations of impulse-wave height in the longitudinal direction. Corresponding correlation-coefficient R2 is 0.94.

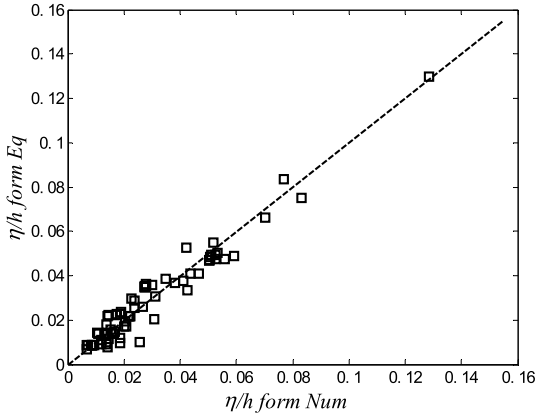

FIGURE 12. Comparison of predicted longitudinal impulse-wave heights by numerical simulation and calculations by Equation (8).

In addition, a similar formula is derived for evaluating the attenuation of an impulse-wave in the lateral direction, as shown in Equation (9):

$$\frac{\eta_r}{h} = 2.324(\frac{H}{h})^{1.02}(\frac{V}{h^3})^{0.776} \sin\beta^{0.449} e^{-\sqrt{0.534}\frac{y}{h}} \quad (9)$$

Fig. 13 depicts the comparison of the predicted impulse-wave heights in the lateral direction and the calculations by Equation (9). It shows that the predicting accuracy of Equation (9) is acceptable, and that the correlation coefficient is 0.97.

D. CASE STUDY

1) STUDY AREA

The Yellow River section in Qinghai province is a typical narrow river-valley reservoir river. The most bank of the Qinghai Yellow River consists of cliffs. The Yellow River is meandering and the water flow condition is complicated.

TABLE 3. The ststic and dynamics scale ratios.

Geometric similarity ratio	Volume similarity ratio	Speed similarity ratio	Time similarity ratio
1:200	$1:200^3$	$1:\sqrt{200}$	$1:\sqrt{200}$

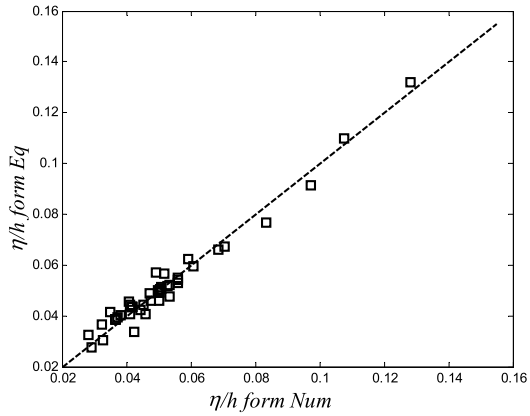

FIGURE 13. Comparison of predicted lateral surge-wave heights by numerical simulation and calculations by Equation (9).

Fig. 14a shows the overall view of the Yellow River section in Qinghai province. The Yellow River Valley concentrates at Longyang Gorge, Laxiwa, Lijiaxia, Zhigang Laka, Kangyang, Gongboxia, Jishixia, and other hydropower stations, forming a cascade of hydropower stations, Fig. 14b. Hence, this region becomes vulnerable to landslide accident. Tangjiaxi, located in Zhexi reservoir, Hunan province, China, was hit by a landslide on July 16, 2014 due to several days of rainfall [22]. The Gongjiafang landslide is located in China's Three gorges reservoir on the Yangtze river, In November 2008, a 380000m^3 slide volume rushed into the water to generate waves [41]. Tafjord is a branch of Stavfjord in western Norway. On April 7, 1934, the impact of possibly 3000000m^3 of rock into Tafjord generated huge waves [17].

2) VALIDATION OF EMPIRICAL FORMULA IN PREDICTINGINITIAL MAXIMUM SURGE HEIGHT

To verify the reliability of our proposed Formula (5) in predicting initial maximum impulse-wave height, we calculated the maximum initial impulse-wave height for four landslide events. and the results were compared with actual measurements and the prediction by Liu's formula [38]:

$$\frac{H_{max}}{h} = 1.17\frac{v}{\sqrt{gh}}(\sin^2\beta + 0.6\cos^2\beta)(\frac{lt}{bh})^{0.15}(\frac{w}{b})^{0.45} \quad (10)$$

where v is the sliding speed, l is slide length, w is slide width, t is slide height, b is river width, and h is water depth.

The established empirical formula uses water depth to make the parameters dimensionless, so that the empirical formula can be extended to a large scale. Table 4 shows the four

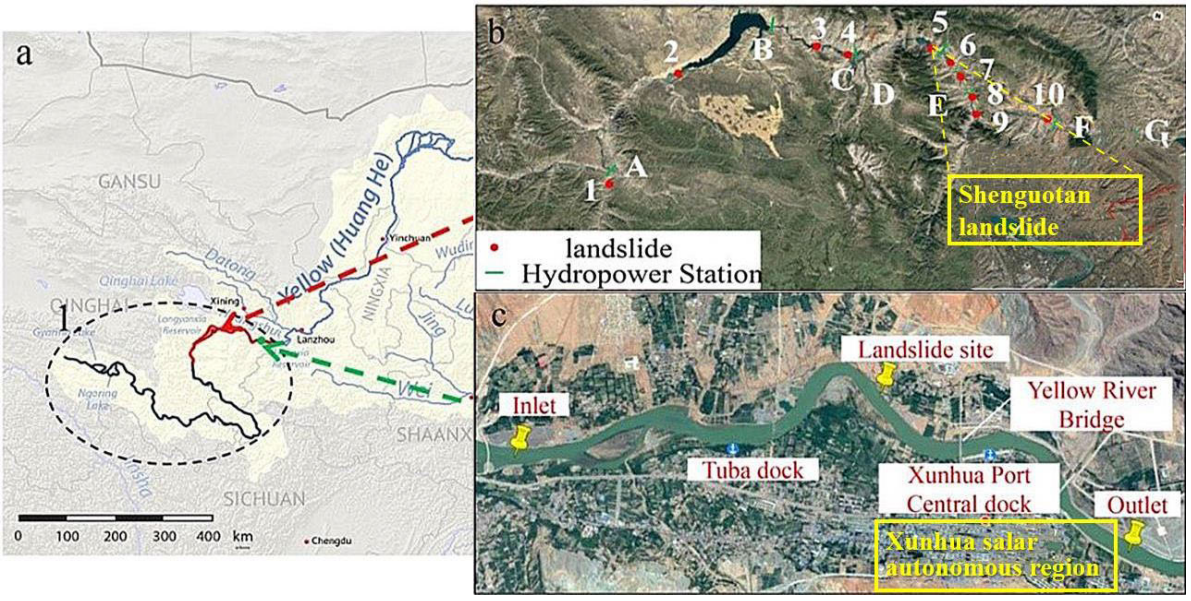

FIGURE 14. Study area. (a) Overall view of Yellow River section in Qinghai province;(b)Hydropower Stations (A: Banduo Hydropower Station, B: Longyang Gorge Hydropower Station C: Laxiwa Hydropower Station, D: LijiaxiaHydropower Station, E: Kangyang Hydropower Station, F: Jishixia Hydropower Station, G: Sigouxia Hydropower Station) and Typical landslide locations (1: Hulietang landslide, 2: Baicitan landslide, 3: Niqiu landslide, 4: Xijitan landslide, 5: Lijiaxia landslide, 6: Shenguotan landslide, 7: Kangyang landslide, 8: Xiazangtan landslide, 9: Dehenglong landslide, 10: Gelongbu early landslide); (c) Location of the landslide event in Jishixia Reservoir area.

TABLE 4. Parameters for each landslide events.

Landslide Event	Length (m)	Width (m)	Thickness (m)	Slide volume (m^3)	Drop height (m)	Still-water depth. (m)	Slide slope (°)
Shenguotan(China)	1700	800	35	4795×10^4	30	16	40
Tangjiaxi(China)	160	67	15	16×10^4	48	30	40
Gongjiafang(China)	98	125	32	38×10^4	82.2	110	53
Tafjord (Norway)	400	130	75	300×10^6	410	220	45

TABLE 5. Comparison of initial maximum surge height of the four landslide events.

Landslide Event	Measured wave (m)	Equation (5) (m)	Equation (10) (m)	The error of equation (5)	The error of equation (10)
Shenguotan(China)	40.26	39.5	38.25	2%	5%
Tangjiaxi(China)	19.5	20.6	21.3	5.6%	9.2%
Gonngjiafang(China)	13.1	12.9	14.4	1.5%	12%
Tafjord (Norway)	62.3	64.4	65.6	3.3%	5.3%

specific landslide events of various parameters. Table 5 lists the comparison of the initial maximum impulse-wave height among measurement, prediction by Liu's formula, and our prediction with Equation (5). As can be seen from table 5 that Equation (5) has a significant improvement over the formula for predicting the maximum initial impulse-wave height. In the Shenguotan landslide, the errors between Equation (5) and Equation (10) and the measured values are 2% and 5%, respectively. In the Tangjiaxi landslide, the errors of Equation (5) and Equation (10) are 5.6% and 9.2%, respectively. In the Gongjiafang landslide, the errors of Equation (5) and Equation (10) are 1.5% and 12%, respectively. In the Tafjord landslide event, the errors of Equation (5) and Equation (10) were 3.3% and 5.3%, respectively. And the average error between Equation (5) and Equation (10) and the measured values is 5.1% and 7.8%, respectively. This comparison

indicates that Equation (5) is reliable in predicting a large leading wave height in narrow river-valley reservoir areas.

IV. CONCLUSION

Landslide-induced impulse waves have become a serious threat to life safety and property intactness, especially in narrow river-valley reservoir areas. This article systematically carried out numerical investigations on the hydrodynamic characteristics of landslide-induced impulse waves in narrow river-valley reservoirs by applying software package FLOW3D. To verify the computational reliability of FLOW3D, new laboratory experiments were performed. The main conclusions are drawn as follows:

1) Compared with previous research on landslides in open-water areas, we conducted a series of experimental work and a 3D numerical simulation on landslide-induced impulse waves in a narrow river-valley reservoir region. The effects of prominent factors such as slide volume, drop height of the slide, slide slope, and still-water depth, on the hydrodynamic characteristics of an impulse-wave have been discussed in detail. It was found that the initial maximum impulse-wave height increased with the slide volume, the drop of the slide, and the slide slope, but decreased with still-water depth. An impulse-wave could be gradually attenuated as it propagates to the surrounding water, and the attenuation rate of the impulse-wave could be greatly affected by slide volume, slide slope, and still-water depth.
2) Based on the simulation results, we derived empirical formulas for predicting the initial maximum impulse-wave height, variations of impulse-wave height, along both longitudinal and lateral directions in the narrow river-valley by performing dimensionless analysis and applying nonlinear regression methods. The accuracy and reliability of the proposed formulas are well-validated by comparing their calculations with corresponding experiment data and simulation results. It can be seen from the formula that as the drop height, and the slide volume, and the landslide angle increase, the initial impulse wave height also increases, which can be found from the numerical analysis results and experimental results. The greater the drop height and the landslide angle can increase the speed of the slider into the water, increase the kinetic energy of the landslide body, the more energy converted into the water body, and the increase in the volume of the landslide, the more the volume of discharged water, the increase in impulse height. When other conditions are constant, the initial impulse wave height decreases as the water depth increases. This is because increasing the water depth is equivalent to reducing the drop height of the slide, which reduces the water inlet speed and kinetic energy of the slide.
3) Four landslide events were used to further verify the reliability of our proposed formula in analyzing the hydrodynamic characteristics of landslide-induced impulse-wave in actual landslide accident. The analytical solutions of the proposed formulas were compared, and were in a good agreement with the field-observation data. It is believed that the findings drawn from this article could greatly enhance our understanding on landslide-induced impulse-wave in narrow river-valley reservoir areas, and our proposed analytical formulas could act as are liable technical tool for evaluating the potential hazards of landslide-induced impulse waves.

ACKNOWLEDGMENT

The authors received funds for covering the costs to publish in open access.

REFERENCES

[1] A. Panizzo, P. De Girolamo, M. Di Risio, A. Maistri, and A. Petaccia, "Great landslide events in italian artificial reservoirs," *Natural Hazards Earth Syst. Sci.*, vol. 5, no. 5, pp. 733–740, Sep. 2005.
[2] R. Vacondio, P. Mignosa, and S. Pagani, "3D SPH numerical simulation of the wave generated by the vajont rockslide," *Adv. Water Resour.*, vol. 59, pp. 146–156, Sep. 2013.
[3] L. Chen, *Experimental Study on Characteristics of Rock-Type Landslide Surge and Impact for Navigable Conditions of the River-Channel Type Reservoir in Mountainous Area*. Chongqing, China: Chongqing Jiaotong Univ., 2014.
[4] D. Gu and D. Huang, "A complex rock topple-rock slide failure of an anaclinal rock slope in the wu gorge, yangtze river, China," *Eng. Geol.*, vol. 208, pp. 165–180, Jun. 2016.
[5] P. Mazzanti and F. V. De Blasio, "The dynamics of coastal landslides: Insights from laboratory experiments and theoretical analyses," *Bull. Eng. Geol. Environ.*, vol. 70, no. 3, pp. 411–422, Aug. 2011.
[6] W. A. N. G. Jian-Feng, "Theoretical analysis to two classic landslide prediction models: Saito's model and Voight's model," *J. Geomech.*, vol. 10, no. 1, pp. 40–50, 2004.
[7] B. C. Mcfall, F. Mohammed, H. M. Fritz, and Y. Liu, "Laboratory experiments on three-dimensional deformable granular landslides on planar and conical slopes," *Landslides*, vol. 15, pp. 1713–1730, Apr. 2018.
[8] F. Mohammed and H. M. Fritz, "Physical modeling of tsunamis generated by three?dimensional deformable granular landslides," *J. Geophys. Res. Oceans*, vol. 118, p. 3221, Nov. 2013.
[9] S. Viroulet, D. Cébron, O. Kimmoun, and C. Kharif, "Shallow water waves generated by subaerial solid landslides," *Geophys. J. Int.*, vol. 193, no. 2, pp. 747–762, May 2013.
[10] G. B. Crosta, S. Imposimato, and D. Roddeman, "Landslide spreading, impulse water waves and modelling of the vajont rockslide," *Rock Mech. Rock Eng.*, vol. 49, no. 6, pp. 2413–2436, 2015.
[11] H. Tan and S. Chen, "A hybrid DEM-SPH model for deformable landslide and its generated surge waves," *Adv. Water Resour.*, vol. 108, pp. 256–276, Oct. 2017.
[12] E. Noda, "Water waves generated by landslides," *J. Waterways, Harbors Coastal Eng. Division*, vol. 96, no. 4, pp. 835–855, 1970.
[13] A. Panizzo, G. Bellotti, and P. De Girolamo, "Application of wavelet transform analysis to landslide generated waves," *Coastal Eng.*, vol. 44, no. 4, pp. 321–338, Feb. 2002.
[14] M. Di Risio and P. Sammarco, "Analytical modeling of landslide-generated waves," *J. Waterway, Port, Coastal, Ocean Eng.*, vol. 134, no. 1, pp. 53–60, Jan. 2008.
[15] V. Heller and W. H. Hager, "Impulse product parameter in landslide generated impulse waves," *J. Waterway, Port, Coastal, Ocean Eng.*, vol. 136, no. 3, pp. 145–155, May 2010.
[16] A. Zweifel, W. H. Hager, and H.-E. Minor, "Plane impulse waves in reservoirs," *J. Waterway, Port, Coastal, Ocean Eng.*, vol. 132, no. 5, pp. 358–368, Sep. 2006.
[17] H. M. Fritz, "Initial phase of landslide generated impulse waves," Ph.D. dissertation, ETH, Zürich, Switzerland, 2002.

[18] F. Zu, P. Wang, J. Xu, and L. Xie, "Experimental study on propagation and attenuation regularity of landslide surge," *Sains Malaysiana*, vol. 46, no. 11, pp. 2061–2074, Nov. 2017.
[19] Y. Yueping, H. Bolin, W. Shichang, and L. Jinhe, "Potential for a Ganhaizi landslide-generated surge in Xiluodu reservoir, Jinsha River, China," *Environ. Earth Sci.*, vol. 73, no. 7, pp. 3187–3196, Apr. 2015.
[20] P. Watts, S. T. Grilli, D. R. Tappin, and G. J. Fryer, "Tsunami generation by submarine mass Failure. II: Predictive equations and case studies," *J. Waterway, Port, Coastal, Ocean Eng.*, vol. 131, no. 6, pp. 298–310, Nov. 2005.
[21] J. Mao, L. Zhao, X. Liu, J. Cheng, and E. Avital, "A three-phases model for the simulation of landslide-generated waves using the improved conservative level set method," *Comput. Fluids*, vol. 159, pp. 243–253, Dec. 2017.
[22] B. Huang, Y. Yin, and S. Wang, "Analysis of the Tangjiaxi landslide-generated waves in the Zhexi Reservoir, China, by a granular flow coupling model," *Natural Hazards Earth Syst. Sci.*, vol. 17, pp. 1–21, May 2017.
[23] J. W. Kamphuis and R. J. Bowering, "Impulse waves generated by landslides," *Coastal Eng.*, vol. 12, pp. 575–588, Jan. 1970.
[24] B. Ataie-Ashtiani and A. Nik-Khah, "Impulsive waves caused by subaerial landslides," *Environ. Fluid Mech.*, vol. 8, no. 3, pp. 263–280, Jun. 2008.
[25] R. H. Li, C. B. Jiang, and B. Deng, "Experimental research on landslide surge wave height and propagation rule of the narrow-river type reservoir in the near-dam area," (in Chinese), *J. Transp. Sci. Eng.*, vol. 32, no. 2, pp. 79–84, 2016.
[26] G. Kim, "Numerical simulation of three-dimensional tsunami generation by Subaerial landslides," M.S. thesis, Texas Aand M Univ., College Station, TX, USA, 2012.
[27] R. Gabl, J. Seibl, B. Gems, and M. Aufleger, "3-D numerical approach to simulate the overtopping volume caused by an impulse wave comparable to avalanche impact in a reservoir," *Natural Hazards Earth Syst. Sci.*, vol. 15, no. 12, pp. 2617–2630, Dec. 2015.
[28] W. Chen, P. Hui, J. Ke, W. Fan, and Y. Shaofei, "Study on the water surge height line of landslide surge of linear river course reservoir based on FLOW-3D," *J. Environ. Sci. Eng. B*, vol. 5, no. 6, pp. 293–298, Jun. 2016.
[29] P. Ghadimi, A. Dashtimanesh, M. Farsi, and S. Najafi, "Investigation of free surface flow generated by a planing flat plate using smoothed particle hydrodynamics method and FLOW3D simulations," *Proc. Inst. Mech. Eng., M, J. Eng. Maritime Environ.*, vol. 227, no. 2, pp. 125–135, May 2013.
[30] D. H. Ko, S. T. Jeong, and J. D. Kim, "Hydraulic characteristic analysis of buoyant flap typed storm surge barrier using FLOW-3D model," *J. Korean Soc. Coastal Ocean Eng.*, vol. 26, no. 3, pp. 140–148, Jun. 2014.
[31] Y. Xiao, W. Wang, and X. Hu, "Numerical simulation of hydraulic performance for portable short-throat flume in field based on FLOW-3D," *Trans. Chin. Soc. Agricult. Eng.*, vol. 32, no. 3, pp. 55–61, 2016.
[32] A. Chandorkar and S. Palit, "Microfluidic devices, droplet dynamics, VOF-based method, TruVOF, FLOW-3D, T-junction, flow patterns, droplet-based microfluidic devices, co-flowing devices,electrowetting, fluid method," *Sensors Transducers J.*, pp. 136–149, 2009.
[33] J. Qiu and X. Fang, "Challenges on three-dimensional simulations of free surface flow," in *World Environmental and Water Resources Congress*, 2009, pp. 1–10. [Online]. Available: https://ascelibrary.org/doi/pdf/10.1061/41036%28342%29279
[34] C. G. Koutitas, "Finite element approach to waves due to landslides," *Proc Asce*, vol. 103, pp. 1021–1029, Jan. 1977.
[35] D. XiaoTang, X. DaLei, Z. Feng, Z. Hui, and Y. Cun, "Numerical simulation of hydraulic characteristic of swirling device based on FLOW-3D software," in *Proc. 7th Int. Conf. Modeling, Identificat. Control (ICMIC)*, Dec. 2015, pp. 1–4.
[36] C. J. Willmott, "On the validation of models," *Phys. Geogr.*, vol. 2, no. 2, pp. 184–194, 1981.
[37] H. M. Fritz, W. H. Hager, and H.-E. Minor, "Near field characteristics of landslide generated impulse waves," *J. Waterway, Port, Coastal, Ocean Eng.*, vol. 130, no. 6, pp. 287–302, Nov. 2004.
[38] Y. L. Liu, *Research on Landslide-Induced Surge in Three Gorges Reservoir Area*. Wuhan, China: China Univ. Geosciences, 2013.
[39] F. Enet and S. T. Grilli, "Experimental study of tsunami generation by three-dimensional rigid underwater landslides," *J. Waterway, Port, Coastal, Ocean Eng.*, vol. 133, no. 6, pp. 442–454, Nov. 2007.
[40] Y. Zhang, D. Li, L. Chen, K. Yin, L. Xiao, X. Fu, T. Glade, and C. Leo, "Numerical analysis of landslide-generated impulse waves affected by the reservoir geometry," *Eng. Geol.*, vol. 266, Mar. 2020, Art. no. 105390.
[41] B. Huang, Y. Yin, G. Liu, S. Wang, X. Chen, and Z. Huo, "Analysis of waves generated by Gongjiafang landslide in Wu gorge, three gorges reservoir, on november 23, 2008," *Landslides*, vol. 9, no. 3, pp. 395–405, Sep. 2012.
[42] V. Heller and J. Spinneken, "Improved landslide-tsunami prediction: Effects of block model parameters and slide model," *J. Geophys. Res., Oceans*, vol. 118, no. 3, pp. 1489–1507, Mar. 2013.
[43] E. Zhao, Y. Tang, J. Shao, and L. Mu, "Numerical analysis of hydrodynamics around submarine pipeline end manifold (PLEM) under tsunami-like wave," *IEEE Access*, vol. 7, pp. 178903–178917, 2019.

BIN DENG received the Ph.D. degree in harbor, coastal and offshore engineering from the Changsha University of Science and Technology, Changsha, Hunan, China, in 2014. He is currently an Associate Professor with the Changsha University of Science and Technology. His current research interests include hydrodynamics, computational fluid dynamics, and wave-structure interaction, with over 40 publications in these areas.

HE TAO received the B.S. degree in water conservancy and hydropower engineering from Bengbu University, Bengbu, Anhui, China. He is currently a Graduate Student of harbor, coastal and offshore engineering with the Changsha University of Science and Technology. His research interest includes computational fluid dynamics.

CHANGBO JIANG received the Ph.D. degree in harbor, coastal and offshore engineering from Tianjin University, Tianjin, China. He is currently a Full Professor with the School of Hydraulic Engineering, Changsha University of Science and Technology, Changsha, China. His current research interests include nearshore hydrodynamic characteristics under coastal dynamic process, computational fluid dynamics, and development of hydrological-hydrodynamic coupling numerical model, with over 300 publications in these areas.

KE QU received the Ph.D. degree in environment water resources from The City College of New York, The City University of New York, USA. He is currently an Associate Professor with the School of Hydraulic Engineering, Changsha University of Science and Technology, Changsha, China. His current research interests include two-phase flow modeling, storm surge modeling, wave-structure interaction, and multi-scale coastal flow model development, with over 30 publications in these areas.